BOONE Technical Note Document # 121, Version 0

# A Study of Photon Arrival Times using a Simple Optical Transport Model

H. A. Tanaka
Princeton University

April 7, 2004

**Abstract**

A simple Monte Carlo simulation is developed to study absorption, scattering and fluorescence in mineral oil. In order to describe these processes, a number of offline measurements are interpreted in a way suitable for incorporation into a Monte Carlo simulation. The predictions of the toy Monte Carlo are compared and checked with other simulations and data where appropriate. Finally, we use the simulation to evaluate the temporal properties of a multiple fluorescence model.

# Contents

**1 Introduction:** **3**

**2 Constructing the Optical Model** **4**
2.1 Extinction . . . . . 4
2.2 Fluorescence . . . . . 5
2.2.1 Fluorescence Spectrum . . . . . 9
2.2.2 Fluorescence Rate . . . . . 11
2.2.3 Fluorescence Lifetime . . . . . 13
2.3 Scattering . . . . . 13
2.4 Absorption: . . . . . 15
2.5 Summary of Optical Model: . . . . . 15

**3 Consistency and Cross Checks:** **17**
3.1 Check of Scattering with boomc . . . . . 17
3.2 Check of Extinction: . . . . . 18
3.3 Crosschecks with Excitation Measurements . . . . . 19

**4 Time Spectrum of** **21**

**5 Effective Fluorescence Spectrum** **21**

**6 Acknowledgments** **21**

**A Novosibirsk Function** **22**

# 1 Introduction:

The propagation of light in the Marcol 7 mineral oil used in MiniBooNE exhibits a remarkably rich array of phenomena. Cherenkov and scintillation photons produced by charged particles passing through the oil are believed to scatter off particles or density fluctuations in the oil and excite atoms and molecules (fluorescence), whereupon light may be re-emitted at a different wavelength. It is also believed that some fraction of the light is absorbed by the oil without further emission (absorption). The rate of each process depends on the wavelength of the light and may result in redirection, wavelength shift and a delay with a characteristic lifetime upon reemission. This suite of processes which govern how a photon propagates through our detector is often referred to as the *optical model*.

Attempts to understand the optical model via data from the MiniBooNE detector have thus far had limited success. In particular, attempts to understand scattering using laser flask data by analyzing late photomultiplier hits have been confounded by uncertainties in the time response of the photomultiplier and possible tails in the emission of light from the laser [5]. Our primary means of understanding scintillation, derived from the time spectrum of late hits in Michel decay electrons reconstructed in the detector, is currently unable to distinguish scintillation from fluorescence. A common theme echoed throughout these studies is the potential for multiple contributions to the late hits. The detector is unable to otherwise discriminate between these contributions without assumptions or external input. In an attempt to overcome these obstacles, a program of offline measurements aimed at isolating particular components of the optical model has been in progress for some time. This program has yielded a wealth of information regarding light transmission [1][3][4], fluorescence [1], and scintillation [6].

A curious feature to emerge from a comparison of the IUCF measurements of scintillation lifetime with scintillation/fluorescence lifetime measurements using Michel decay electrons in the MiniBooNE detector is a discrepancy in the observed lifetime: the former measures an $18.6 \pm 1.0$ ns, whereas the latter suggests a much longer lifetime between 30 and 50 ns. The currently favored hypothesis assumes that the underlying scintillation/fluorescence mechanisms are identical in the two cases. With the observation that the short ($\sim$ 290 nm) wavelength spectrum of fluorescence implies a short pathlength in the mineral oil, light may fluoresce or scintillate repeatedly in an extended volume of mineral oil. The difference in the observed lifetimes results from the large difference in pathlength from production to detection in the two cases; a few centimeters in the IUCF measurement, typically a few meters at MiniBooNE. In the latter case, the result is an "effective" lifetime that is longer than the fundamental lifetime that governs a single fluorescence/scintillation event.

The primary goal of this study is to investigate the viability of this reemission model in reconciling the different lifetimes observed in the IUCF and Michel electron measurements. Currently, the MiniBooNE detector Monte Carlo (boomc) is unable to simulate multiple delayed emission. As a result, an independent simulation, hereafter referred to as the toy Monte Carlo or toy MC, has been developed. To meaningfully study the multiple emission process, the study also includes an attempt to interpret the available data on Marcol 7 optical properties to construct an optical model incorporating scattering, absorption and fluorescence. We start with a discussion of how currently available data is used to construct this model. We continue by verifying the predictions to the model where boomc and external measurements allow comparison. Finally, we analyze the time spectrum predicted by the multiple reemission model.

# 2 Constructing the Optical Model

The optical model for the toy Monte Carlo consists of three processes: absorption, fluorescence, and scattering. For each process, the rate (typically in the form of an interaction length), output spectrum, and lifetime of any reemission must be specified. In constructing the optical model for the toy MC, we use the following information:

- **Index of refraction:** We use Hans Otto Meyer's measurements and parametrization of the index of refraction described in Equation 1 of Reference [2]. Using Equations 10 and 11, we obtain the group velocity of light. The index of refraction and group velocities used in this model are shown as a function of wavelength in Figure 1.
- **Extinction:** By extinction, we mean any process which alters the wavelength or direction of the incident. In our case, extinction represents the sum of the processes under consideration: scattering, fluorescence and absorption. There are two measurements of the overall extinction of light as it passes through the mineral oil, one based on the Alabama [3] and Cincinnati [4] testers used in the WIN baseline, and the other from transmission measurements through a 1 cm cuvet performed by Anna Pla and Shannon [1]. These measurements are likely to be valid in different ranges of wavelength. We describe in Section 2.1 how they are combined to produce a single model of extinction.
- **Fluorescence:** As mentioned earlier, Anna Pla and Shannon have provided a wealth of data on fluorescence, mainly in the form of the observed fluorescence spectrum for a given input wavelength (spectrum measurements) and the amount of fluorescence observed at a given output wavelength as a function of input wavelength (excitation measurements). We discuss in Section 2.2 how this data is interpreted.
- **Scattering:** Studies of laser flask data have indicated that the observed late tail in the corrected time distribution can be interpreted as scattering with a length of $\sim 28$ meters at 397 nm wavelength. We discuss in Section 2.3 how this information is generalized to describe scattering at all wavelengths.

## 2.1 Extinction

The transmission measurements from Reference [1] as a function of incident wavelength obtained from two samples of Marcol 7 mineral oil in a 1 cm cuvet are shown in the top two plots of Figure 2. The black curves are the raw measurements. The red "corrected" curve is obtained by rescaling the raw curve to level off at approximately 100% transmission assuming that the transmission should be nearly complete at long wavelengths. In the bottom two figures, the transmission measurement at each wavelength is converted to an extinction length $L_e$ using the relation:

$$L_e(\text{cm}) = -1/\log(\text{Transmission(percent)}/100) \tag{1}$$

assuming a pathlength of 1 cm through the oil. Since $L_e$ is not defined for values of transmission above 100%, we calculate $L_e$ up to the first measurement that exceeds 100%.
The transmission measurements using the Alabama and Cincinnati tester have been summarized in the WIN baseline model shown as the the black curve in the bottom plots of Figure 2. These can be compared with the extinction lengths inferred from the 1 cm cuvet measurements (blue and

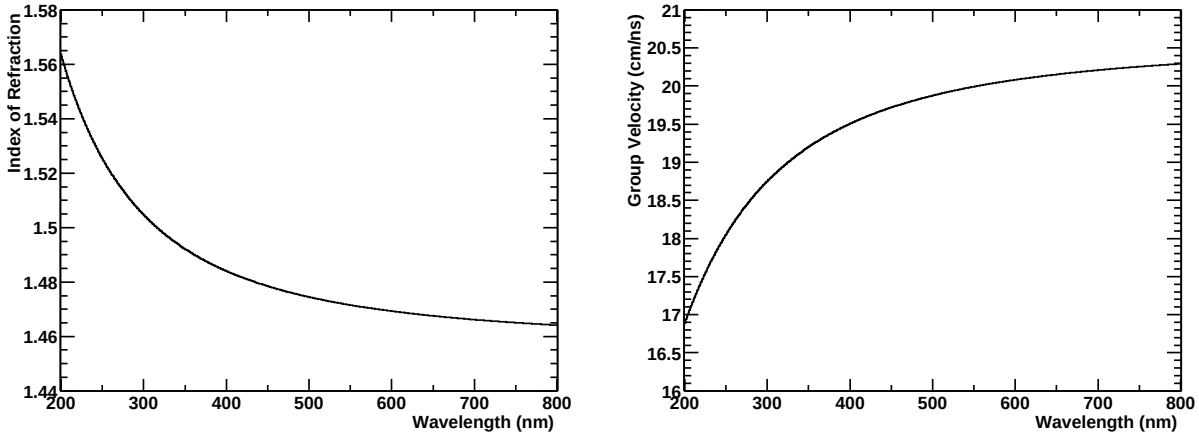


Figure 1: Left: Index of refraction versus wavelength used in toy MC. Right: Group velocity versus wavelength used in toy MC. Both are based on parametrizations from Reference [2].

red).
The extinction lengths based on the original corrected measurements are shown in red for the two samples of oil. It can be seen that above 325 nm (extinction lengths of greater than a few meters) there is a significant discrepancy with the WIN model. This discrepancy has been noted by Gerry Garvey [7]. To resolve this discrepancy, we note that the validity range of these two measurements are quite different: it is likely that the Alabama/Cincinnati measurements are reliable at longer extinction lengths (a few meters) and invalid at short extinction lengths ($< 1$ m) where the 1 cm cuvet measurements are likely to be more reliable. The somewhat arbitrary correction required to bring the transmission measurements to 100% at long wavelengths implies that the reliability of the transmission measurements is questionable as they approach 100%, around 325 nm. In an attempt to reconcile the two measurements, the corrected 1 cm cuvet measurements are scaled by 1.02, resulting in the blue curves in Figure 2. By comparing with the red curves, it can be seen that this is a minor perturbation to the transmission measurements below 325 nm (smaller than the uncertainty implied by the original correction), and allows the two extinction length models to be compatible between 300 and 325 nm. This second correction is arbitrary, motivated only by the desire to have a extinction model that is continuous across the wavelengths of interest, while allowing each model to hold ground in their respective range of expected validity. The extinction length model used in the toy Monte Carlo thus uses the values inferred from the 1 cm cuvet measurements from the second sample of Marcol 7 mineral oil (another arbitrary choice), scaled by 1.02, up to 325 nm, and the WIN baseline model for higher wavelengths.

## 2.2 Fluorescence

A complete fluorescence model specifies for each input wavelength the rate of fluorescence per unit pathlength, the spectrum of the output light, and the time delay of the emitted light. A more comprehensive model would incorporate wavelength-dependent delays by having multiple fluorescence mechanisms, each with a characteristic output spectrum and lifetime.

The construction of the fluorescence model brings together three measurements performed by

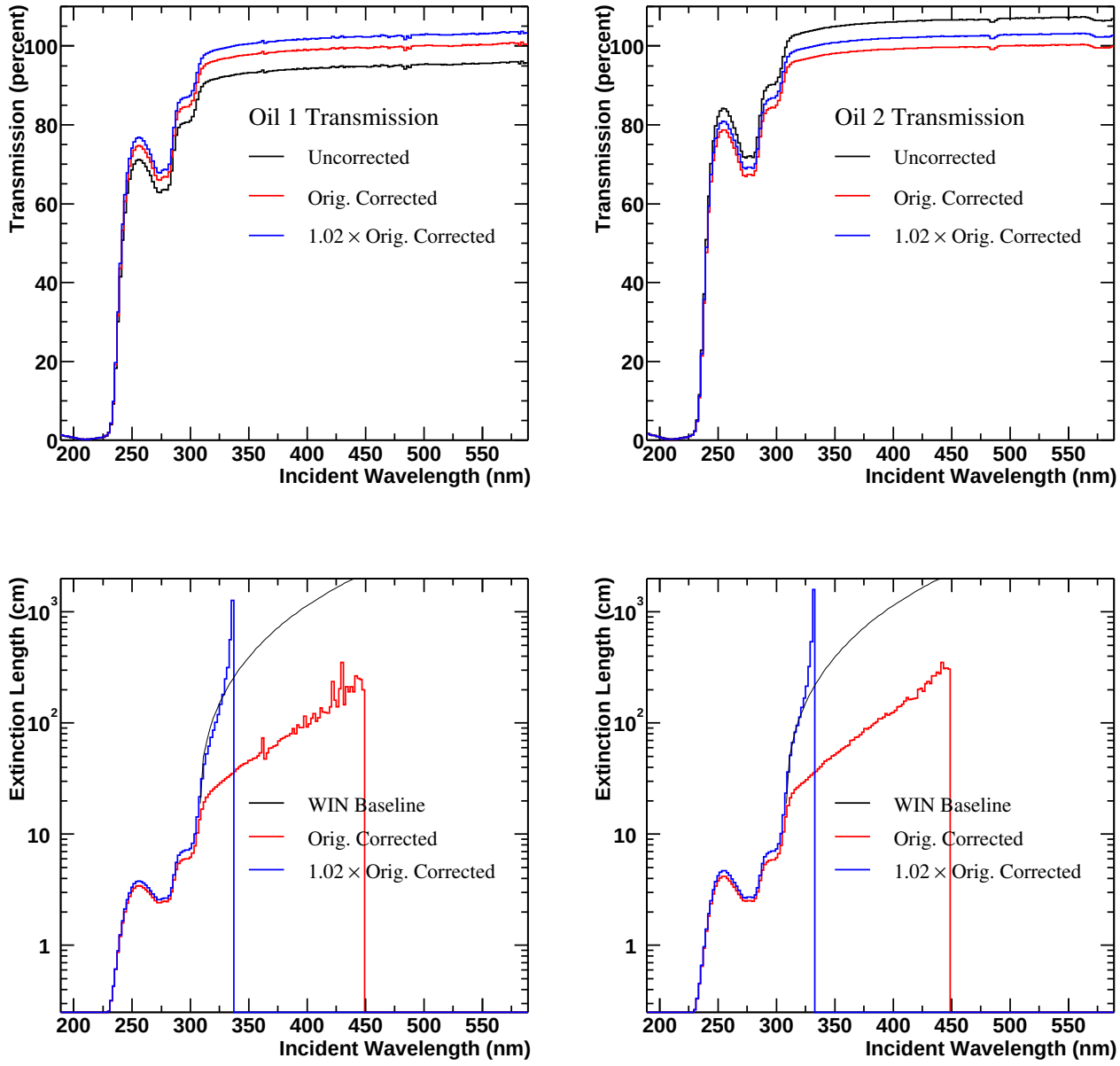


Figure 2: Top left: Transmission versus wavelength for a sample of Marcol 7 oil. Top right: Same for a second sample. Bottom left: Inferred extinction length for first sample compared to WIN baseline model based on data from Alabama and Cincinnati testers. Bottom right: same for second sample.

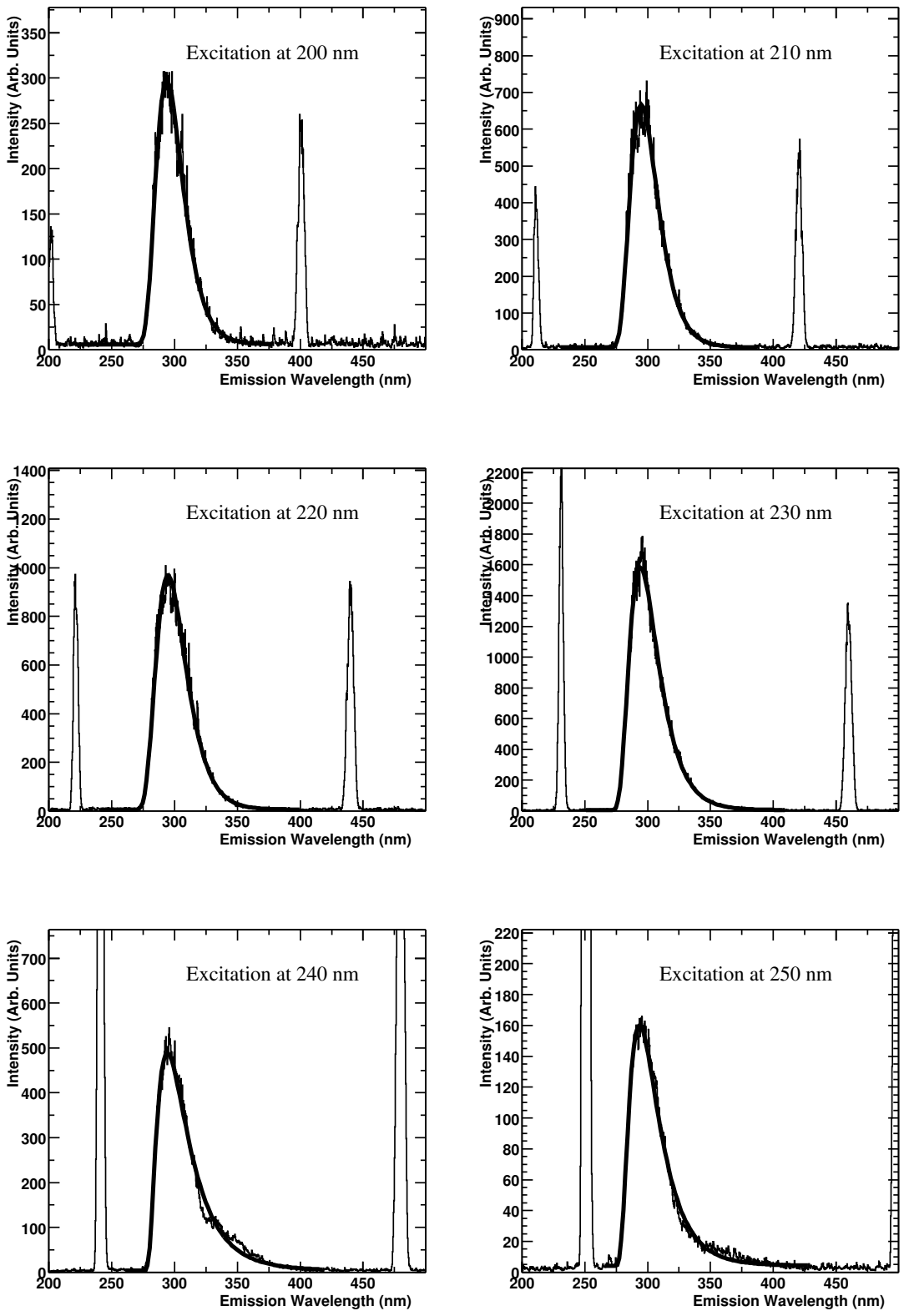


Figure 3: Spectrum of fluorescence at input wavelengths between 200 and 250 nm from Reference [1]. The Novosibirsk function with a flat background is used to fit each spectrum .

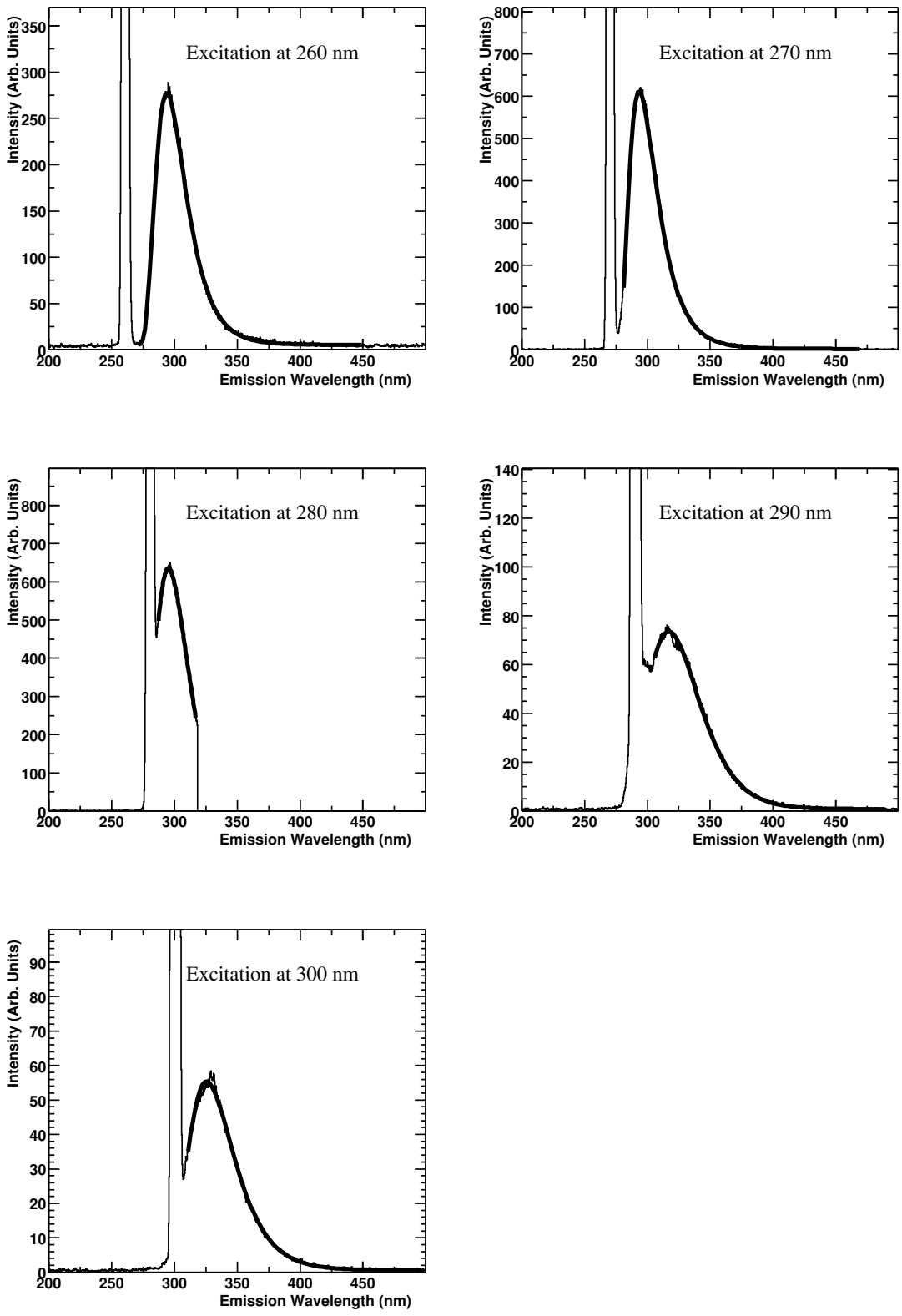


Figure 4: Spectrum of fluorescence at input wavelengths between 260 and 300 nm from Reference [1]. The Novosibirsk function with a flat background is used to fit each spectrum .

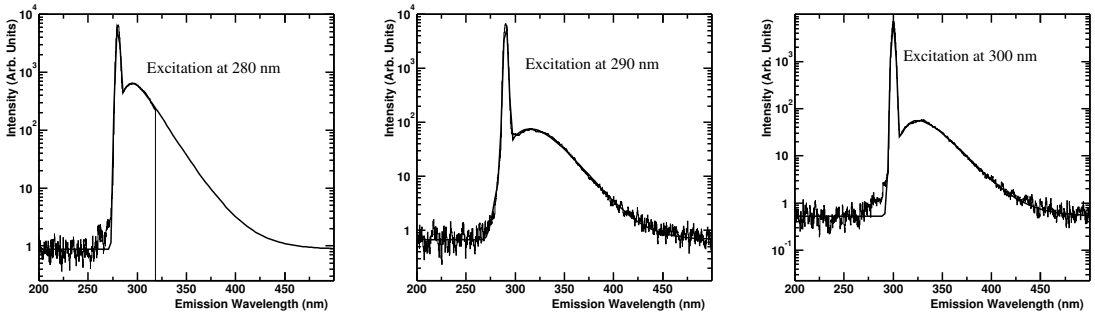


Figure 5: Spectrum of fluorescence at input wavelengths between 280 and 300 nm from Reference [1]. The Novosibirsk function with a flat background is used to fit the spectra. An additional Gaussian component is included to account for the reflected/scattered incident light.

Anna Pla and Shannon:

- Spectrum measurements: the spectrum of the fluorescence is measured at input wavelengths between 200 and 300 nm, nearly the entire relevant range.
- Excitation measurements: the relative intensity of fluoresced light at six wavelengths is measured as a function of the wavelength of the incident light. This provides information on the rate of fluorescence as a function of input wavelength.
- Transmission measurements: Features of the transmission measurement (see Section 2.1) that coincide with features in the excitation measurements provide a rough measure of the overall rate of fluorescence. In addition, the extinction lengths inferred from the transmission measurements are used to correct for the non-negligible extinction of light across the one centimeter cuvets used in these measurements.

### 2.2.1 Fluorescence Spectrum

The fluorescence spectrum measurements are shown in Figures 3 (200–250 nm input wavelength) and 4 (260–300 nm input wavelength). Each spectrum is fit to the Novosibirsk function (see Appendix A), a pseudo-Gaussian function with a peak, width and tail parameter. A flat background component is also included. The fits describe the spectra well, with the exception of the 240 and 250 nm spectra, where the tail deviates from the parameterized form. The data for the 280 nm incident wavelength spectrum is incomplete; the available data is shown with the fit extending over over the wavelengths where data exists.
For incident wavelengths above 280 nm, the peak from the scattered and reflected light (observed at the incident wavelength) starts to overlap with the fluorescence spectrum. In order to account for possible interference, these distributions are refit with an additional Gaussian component to account for this contribution. The fitted distributions for 280, 290 and 300 nm incident wavelength are shown in Figure 5. While the function for the 280 nm spectrum extends beyond the 317 nm (where the data ends), the fit extends only over the range where the data exists. The values of the parameters obtained from the fit are shown in Figure 6. The top plot shows the fitted peak

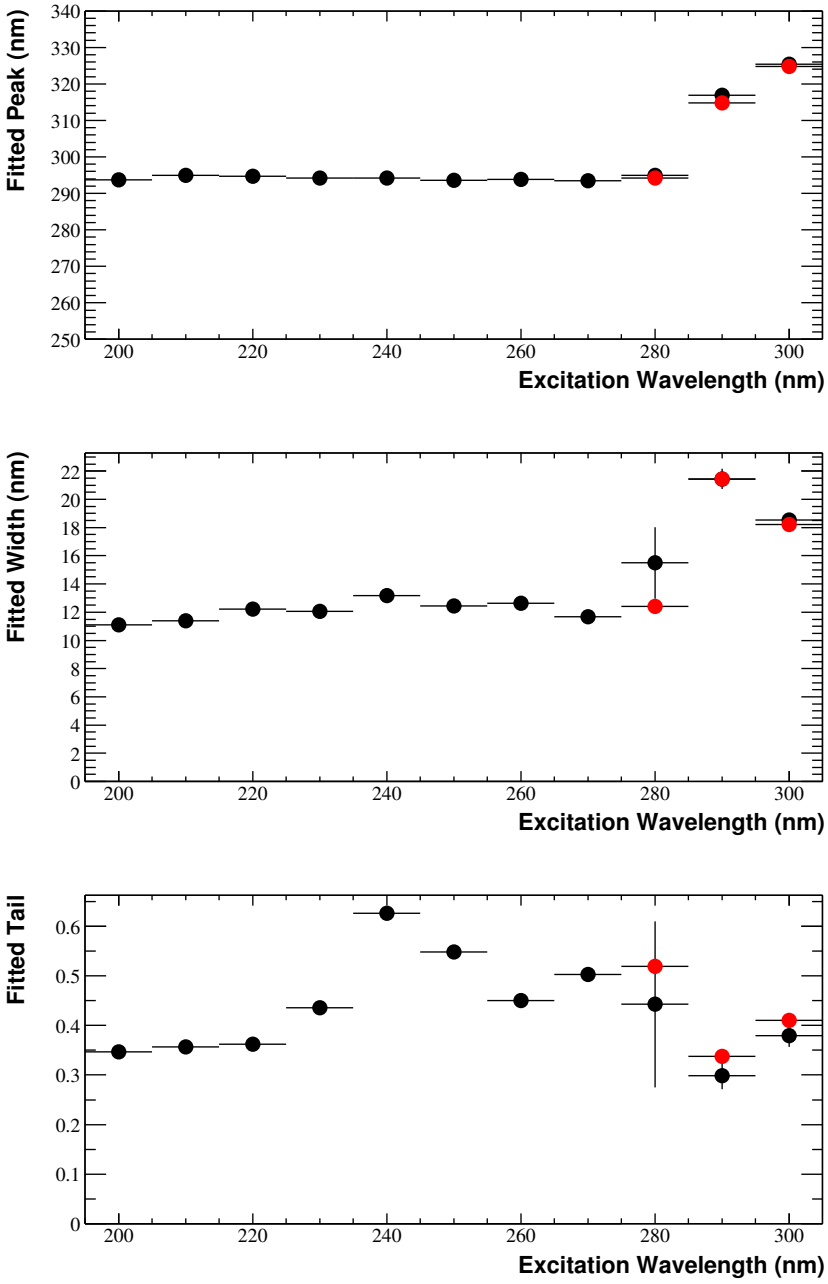


Figure 6: Parameters resulting from fitting the fluorescence spectra to Novosibirsk function as a function of input wavelength. Top: Fitted peak value. Middle: Fitted width. Bottom: Fitted tail parameter. The three red points at 290 and 300 nm are the results from a fit that includes a Gaussian component to describe the reflected/scattered incident light.

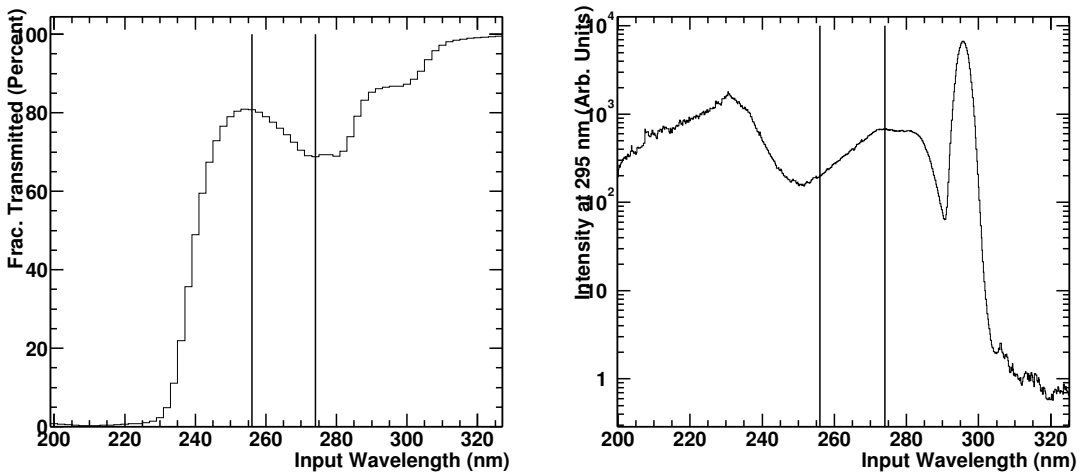


Figure 7: Top: Transmission versus wavelength. Bottom: Excitation measurements for 295 nm output wavelength. The vertical lines indicate 256 nm and 274 nm input wavelengths.

position of the Novosibirsk function, the middle plot shows the fitted width, and the bottom shows the fitted tail parameter. The black points are obtained from the Novosibirsk plus background fits, while the red points are obtained after including the additional Gaussian component. The parameter values obtained in the two versions of the fit for the 280, 290 and 300 nm spectra are consistent. The red points are used at these wavelengths for all studies described in this document. The mean and width of the fits appear to be relatively constant between 200 and 270 nm in incident wavelength, while the tail parameter shows considerable variation. It appears that a qualitative change in the spectrum occurs around 240 and 250 nm, where the fits are poor, resulting in a large change in the tail parameter. As the incident wavelength approaches and exceeds the typical peak value of the spectra, the spectrum must change to ensure that the output wavelength is longer than the incident wavelength. In this region ($>$ 280 nm incident wavelength), the fitted peak position rises steadily to shift the distribution above the incident wavelength.
With these parameterized distributions, the fluorescence spectrum at any input wavelength between 200 and 300 nm is obtained by interpolating the parameters of the Novosibirsk function. The wavelength of an outgoing photon from a fluorescence event can be randomly drawn from the resulting function. For input wavelengths of greater than 300 nm, the peak parameter is extrapolated linearly from the 290 nm and 300 nm points, while the width and tail parameters are fixed to the values obtained from the 300 nm spectrum.

### 2.2.2 Fluorescence Rate

Unfortunately, there is no explicit information on the absolute rate of fluorescence in the spectrum and excitation measurements. A hint, however, is provided by comparing the transmission and excitation measurements, as shown in Figure 7 for 295 nm output wavelength. The drop in transmission around 270 nm roughly coincides with an increase in the rate of fluoresced light at about the same incident wavelength. One can speculate that the two are related, or even equate the two features by hypothesizing that the deficit in outgoing light between 256 and 274 nm in

the transmission measurement has gone to the increased fluorescence observed in the excitation measurements. This relation allows us to translate the arbitrary normalization of the excitation measurement to a fraction of incident light lost to fluorescence. The model can be generalized by introducing a parameter $m$, the fraction of extinction actually going to fluorescence. The only real information we are gleaning from this hypothesis is that $m \sim \mathcal{O}(1)$. The relation can can be expressed as:

$$m \times (T(\lambda_1) - T(\lambda_2)) \approx \epsilon(\lambda_2, \lambda_o) \times \frac{\int \phi(\lambda_2, \lambda) d\lambda}{\phi(\lambda_2, \lambda_o)} - \epsilon(\lambda_1, \lambda_o) \times \frac{\int \phi(\lambda_1, \lambda) d\lambda}{\phi(\lambda_1, \lambda_o)} \tag{2}$$

where $\lambda_1$ and $\lambda_2$ are 256 and 274 nm, respectively, $T(\lambda)$ is the measured transmission at wavelength $\lambda$, $\epsilon(\lambda_i, \lambda_o)$ is the observed fluorescence intensity for incident wavelength $\lambda_i$ at output wavelength $\lambda_o$ from the excitation measurements, while $\phi(\lambda_i, \lambda_o)$ is the fluorescence intensity at output wavelength $\lambda_o$ for input wavelength $\lambda_i$ determined from the spectrum measurements. In principle, $\epsilon$ and $\phi$ are the same function. In practice, the former is discrete in $\lambda_o$ and continuous in $\lambda_i$, while the reverse is true for the latter. The two measurements also have different arbitrary normalizations.
On the right side of the equation, the first term normalizes the fluorescence observed at $\lambda_o$ with input wavelength $\lambda_2 = 274$ nm to the total fluorescence (the integral) based on the relative output intensity at $\lambda_o$ observed in the spectrum measurement at input wavelength $\lambda_2$. The second term does the same at $\lambda_1 = 256$ nm. Thus, the difference in total fluorescence inferred by the excitation measurements (via the spectral measurements to normalize the intensity at a particular output wavelength to the total fluorescence), is equated to the difference in transmission scaled by $m$.
One further correction, particularly relevant at small wavelengths, is made to account for the extinction of light across the 1 cm cuvet in the fluorescence measurements. As seen from Figure 2, the transmission measurements imply that the extinction lengths approaches and then falls below one centimeter at input wavelengths shorter than 300 nm. One can infer that the intensity of incident light at these wavelengths decreases significantly as one traverses across the cuvet, producing less fluorescence. The intensity is given by an exponential decay characterized by the extinction length $L_e$ (*i.e.* $e^{-x/L_e}$) The fraction of incident light converted to fluorescence implied by Equation 2 should be corrected account for the decreasing intensity of light by dividing by the average intensity of light through the cuvet ($1 - e^{-L_c/L_e}$, where $L_c$ is the pathlength through the cuvet) relative to the initial intensity. Finally, all the pieces can be assembled to translate the intensity observed in the excitation measurements into a fraction of incident light fluoresced $\mathcal{F}$, up to an overall factor $m$:

$$\begin{aligned} \mathcal{F}(\lambda_i) \quad \approx \quad & m \times \left(1 - e^{-L_c/L_e}\right) \times \epsilon(\lambda_i, \lambda_o) \times \frac{\int \phi(\lambda_i, \lambda) d\lambda}{\phi(\lambda_i, \lambda_o)} \times \\ & (T(\lambda_1) - T(\lambda_2)) \times \left[\epsilon(\lambda_2, \lambda_o) \times \frac{\int \phi(\lambda_2, \lambda) d\lambda}{\phi(\lambda_2, \lambda_o)} - \epsilon(\lambda_1, \lambda_o) \times \frac{\int \phi(\lambda_1, \lambda) d\lambda}{\phi(\lambda_1, \lambda_o)}\right]^{-1} \end{aligned} \tag{3}$$

With six separate excitation measurements, one has six independent measurements of the fluorescence rate across most of the relevant input wavelengths. The excitation measurements and fluorescence lengths ($L_f$) inferred from Equation 3 with $m = 0.5$ are shown in Figure 8. A number of issues are apparent:

- While a number of qualitative similarities are found across the some or all the measurements, the method outlined above does not give consistent results for each excitation measurement.

- The validity of each excitation measurement becomes questionable as one approaches the output wavelength, where reflection and scattering of the input light becomes dominant. We assume on physical grounds that the measurements are not valid at input wavelengths greater than the output wavelength.

- Where the curves disagree, one must chose a particular curve. Below 275 nm, we give preference to the 295 nm excitation measurement, based on the observation that the peak of the fluorescence spectra are typically close to 295 nm, and that the intensity of the fluorescence at the peak probably gives a better indication of the total fluorescence rate than a measurement on the tail of the spectrum.

- Between 275 and 295 nm, the default model uses the lengths inferred from the 310 nm excitation measurements, which lies roughly in between the span of the different measurements. As alternatives, we use the 295 nm curve and the 340 nm curve, which lie at the extremes. The three models are shown in Figure 9

- The measurements indicate that there may be significant fluorescence at incident wavelengths of 300 nm and above. We have no reliable measurements beyond $\sim$ 320 nm. For incident wavelengths 310 nm and above, we use a parametrization:

$$L_f(\text{cm}) = 207971 - 1387.22 \times \lambda(\text{nm}) + 2.31303 \times \lambda^2(\text{nm}) \tag{4}$$

  to describe the fluorescence length, based on a fit of the fluorescence lengths calculated from the 340 nm excitation measurement between 310 and 320 nm.

- Depending on the choice of $m$, the fluorescence rate may exceed the extinction rate. This occurs if $m = 1$. The choice of $m = 0.5$ results from selecting an arbritrary number less than one where this unphysical situation does not occur.

While there are some ambiguities and discrpencies that have been solved arbitrarily, we now have a model that specifies the rate of fluorescence as a function of incident wavelength. We will investigate other solutions to the ambiguities later.

### 2.2.3 Fluorescence Lifetime

As mentioned in Section 1, the time distribution of scintillation produced by protons traversing Marcol 7 mineral oil was observed to have a lifetime of $18.6 \pm 1.0$ ns. Measurements of scintillation lifetime in neutrino events and Michel decay electrons in the MiniBooNE detector have yielded values of 30–50 ns. In this study, we will assume that single fluorescence events have a lifetime of 18.6 ns, and determine the "effective" lifetime resulting from multiple fluorescence events.

## 2.3 Scattering

It is currently believed that light in the detector is scattered either by particles or density perturbations in the mineral oil. The latter contribution, with the assumption that the size of the perturbations are smaller than the wavelength of light, can be estimated using the Einstein-Smoluchowski equation for the scattering coefficient:

$$\alpha_s = \frac{1}{6\pi n}\left(\frac{\omega}{c}\right)^4 \left|\frac{(\epsilon-1)(\epsilon+2)}{3}\right| \cdot nkT\beta_T \tag{5}$$

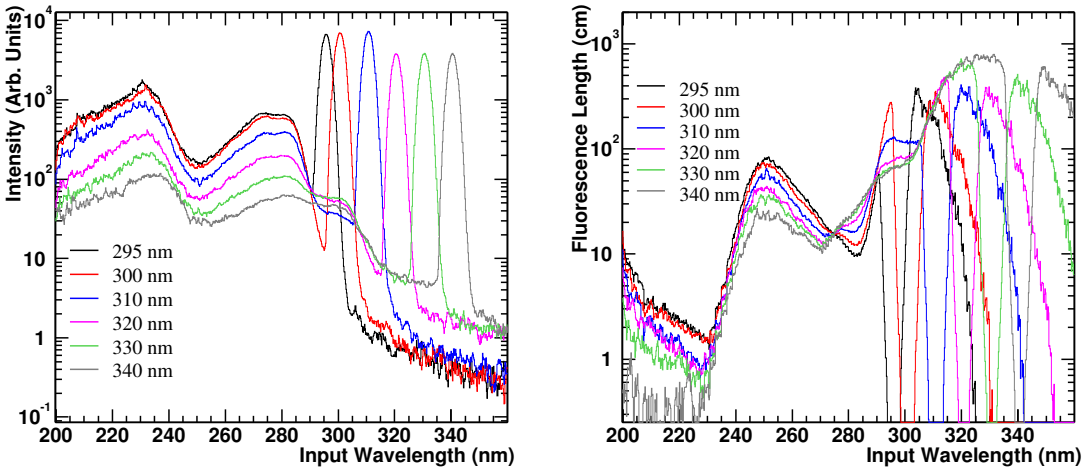


Figure 8: Left: Excitation measurements at output wavelengths of 295, 300, 310, 320, 330 and 340 nm. Right: Fluorescence lengths inferred from Equation 3 with $m = 0.5$.

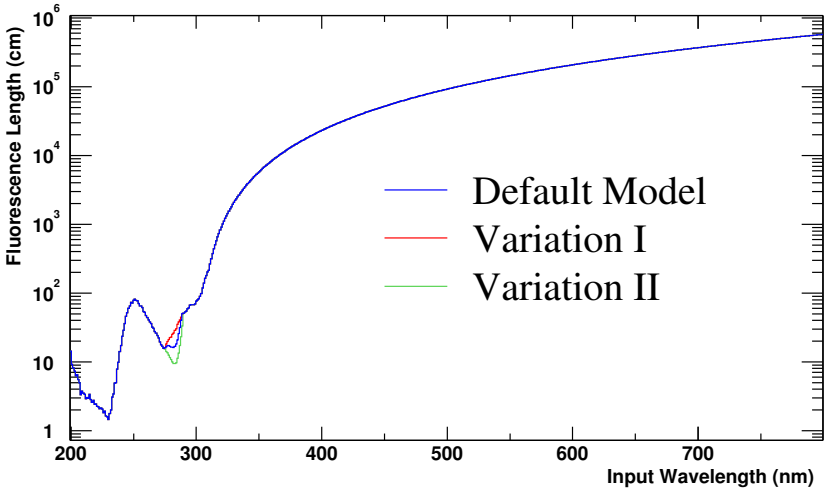


Figure 9: Three models of fluorescence lengths in the 275-290 nm region. The blue curve is the default model and the red and green curves are two alternatives described in the text.

(Equation 9.118 in Reference [8]), where $\omega$ is the angular frequency of the incident light, $\epsilon$ is the dielectric constant of the medium, $n$ is the number density and $T$ is the temperature. The magnitude of the density fluctuations are estimated thermodynamically using the isothermal compressibility $\beta_T$, with the corresponding variation in the index of refraction estimated using the Clausius-Mossotti relation (see Equation 4.70 in Reference [8]). The scattering coefficient (related to the scattering length by $\alpha_s = n\sigma = 1/L_s$) shows the $1/\lambda^4$ dependence derived by Rayleigh to describe scattering in the atmosphere. This wavelength dependence is universal in cases where the size parameter $x = 2\pi nr/\lambda$ is small, where $n$ is the index of refraction of the medium and $r$ is the radius of the scattering elements. This corresponds to the case where the scattering elements are small compared to the wavelength of light. The angular distribution in this limit is flat in $\cos\theta$ for light scattered into the plane orthogonal to the polarization and $\cos^2\theta$ in the plane parallel to the polarization, where $\theta$ is the polar angle between the scattered and incident light. Scattering in this regime is often generically referred to as *Rayleigh scattering*, regardless of whether the scattering elements are density perturbations or discrete particles in the medium.
The rate of scattering in the mineral oil has been studied using center flask laser data at 397 nm assuming an extinction length of 14.4 meters derived from the Alabama/Cincinnati testers. With these assumptions, the late tail in the corrected time distribution is consistent with half of the extinction going to scattering, *i.e.* $L_s = 28.8$ meters. An estimate of Rayleigh scattering using Equation 5, using a measurement of $\beta_T$ described in Reference [9], one derives $L_s = 47.62$ meters at 400 nm [10]. At face value, this indicates that there are other sources of scattering in the mineral oil beside density perturbations.
If we assume that whatever additional sources of scattering are small relative to the incident wavelength, we can use the Rayleigh wavelength dependence and dipole angular spectrum. The scattering model is thus:

- Set the scattering length at 397 m to $L_s = 28.8$ meters
- Assume that $L_s \propto \lambda^4$
- Assume the dipole $(1 + \cos^2\theta)$ angular dependence for unpolarized light.

We hope that future measurements will enhance our understanding of the nature of scattering in the mineral oil.

## 2.4 Absorption:

The process of absorption in mineral oil, whereby incident light disappears without further emission, has not been studied directly. Since we have assumed that the overall extinction at any wavelength consists of fluorescence, scattering and absorption, we can infer the absorption length $L_a$ by:

$$L_e(\lambda)^{-1} = L_f(\lambda)^{-1} + L_s(\lambda)^{-1} + L_a(\lambda)^{-1} \tag{6}$$

at any incident wavelength $\lambda$.

## 2.5 Summary of Optical Model:

We summarize the optical model as follows:

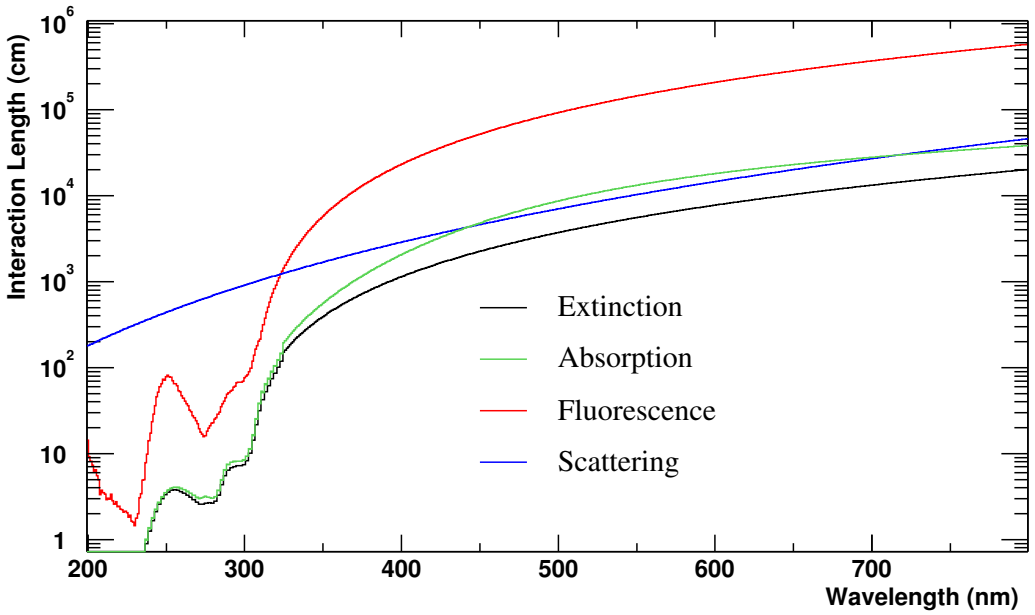


Figure 10: Interaction lengths for the default optical model for the toy Monte Carlo simulation.

- At each wavelength, light may undergo three processes: fluorescence, scattering and absorption.
- For the overall extinction, transmission measurements from 1 cm cuvets and the Alabama/Cincinnati tester are used. The former are used between $200 - 320$ nm, and the latter beyond 320 nm reflecting their expected range of validity. The 1 cm cuvet measurements are scaled by 1.02 to bring the two sets of measurements into agreement in the intermediate region ($\sim 320$ nm).
- The fluorescence rate is estimated by normalizing the excitation measurements assuming that the decrease in transmission at 256-274 nm can be attributed to the increase in fluorescence observed in this interval. The 295 nm excitation measurement is used for 200-290 nm incident wavelengths, the 340 nm measurement for 290-320 nm, and a linear extrapolation used for wavelengths beyond 320 nm. The wavelength of the output light is drawn from parametrizations of the spectrum measurements. The lifetime of the delay is assumed to be 18.6 ns.
- The scattering rate is extrapolated from center flask laser measurement at 397 nm wavelengths using the $1/\lambda^4$ dependence and $1 + \cos^2\theta$ angular dependence, with the assumption that the scattering elements are small relative to the wavelength of incident light. The scattering rate at 397 nm, however, is inconsistent with density perturbations, as estimated by the Einstein-Smoluchowski equation and a measurement of the isothermal compressibility.
- The absorption rate is calculated by attributing to absorption the difference between the total extinction from the sum of fluorescence and scattering.

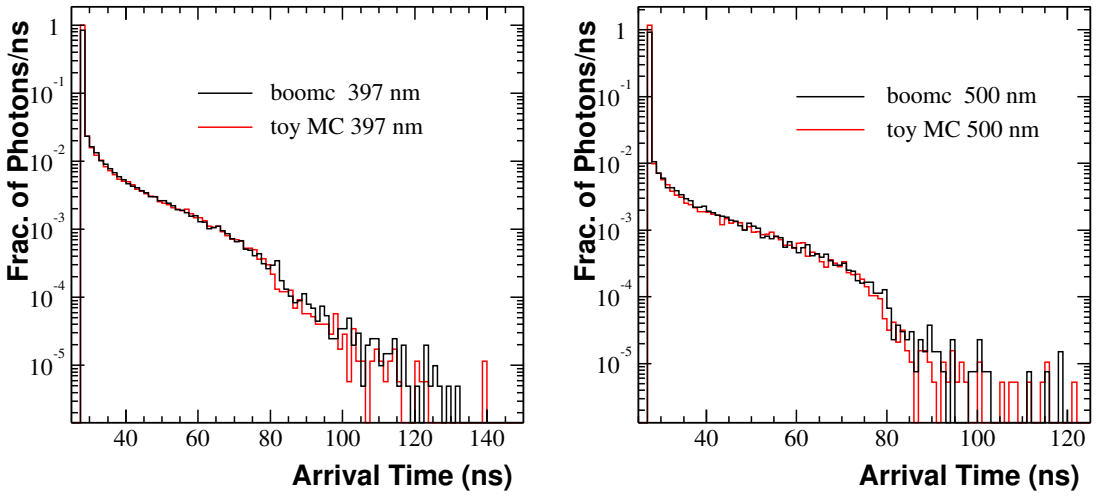


Figure 11: Comparison of toy Monte Carlo and boomc predictions for arrival time of 397 nm (left) and 500 nm (right) light produced at the center of the MiniBooNE detector.

The rate of each process as a function of wavelength, in the form of interaction lengths, are shown in Figure 10.

# 3 Consistency and Cross Checks:

A few checks can performed with the toy Monte Carlo to see that the optical model behaves as expected. We make the following comparisons and consistency checks:

- **Scattering:** We generate photons at the center of a 540 cm sphere and compare the arrival time of the photons at the surface at the sphere to a simulation of center laser flask data using boomc.
- **Extinction:** We simulate the 1 cm cuvet transmission measurements by generating a monoenergetic beam of photons incident along the $z$ axis into a 1 cm diameter sphere centered on the origin. The fraction of transmitted photons (that are not absorbed or scattered and do not fluoresce) is compared with the transmission measurements at the same wavelength.
- **Fluorescence:** We simulate the 1 cm excitation measurements by generating photons with a flat wavelength distribution incident along the $z$ axis into a 1 cm diameter sphere centered on the origin. At a fixed wavelength of outgoing light outside of the forward peak, we evaluate the spectrum of incident light. This is compared to the excitation measurements at the same wavelength.

## 3.1 Check of Scattering with boomc

In this check, we simulate the MiniBooNE detector as a 540 cm sphere and the center laser flask by generating monoenergetic photons isotropically from the center of the sphere. We account for a

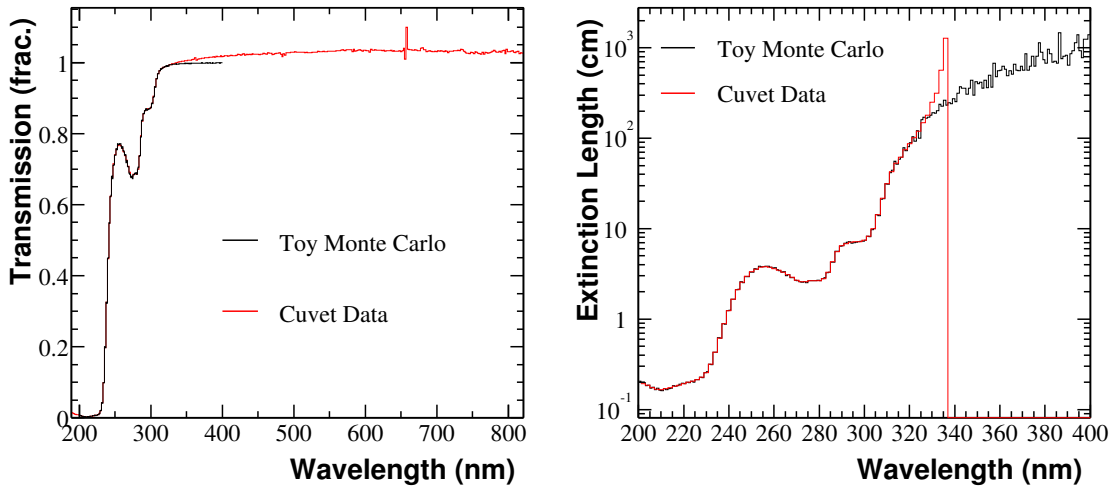


Figure 12: Comparison of toy Monte Carlo predictions for transmission through 1 cm of Marcol 7 mineral oil compared with transmission measurements in a 1 cm cuvet.

number of differences between this representation and boomc:

- The toy Monte Carlo does not explicitly simulate the photomultipliers. The number of photons generated per event is roughly corrected to account for the surface coverage and photocathode efficiency of the photomultipliers. In boomc, we also remove the angular dependence of the photocathode efficiency.
- Reflections are not simulated in the toy Monte Carlo. Reflections are turned of in boomc to match this configuration.
- Fluorescence of optical photons is not simulated in boomc. To account for this, the fluorescence in the toy Monte Carlo is turned off.

With these modifications, 397 nm and 500 nm light is produced in each Monte Carlo simulation. The arrival time of the photomultipliers at 540 cm in the toy Monte Carlo, or at the PMT face in boomc are shown in Figure 11.
While the tail of late light agrees well in the two cases, more prompt light is seen in the toy Monte Carlo relative to the scattered light than in boomc. We believe that this is due to the change in the effective solid angle coverage of the photomultipliers as the source of light moves from the center of the sphere/detector. The result of this change is that boomc, with properly simulated photomultipliers, has a higher relative efficiency for reconstructing scattered light, which behaves as an off-center source of light. The proper simulation of the photomultiplier geometry is beyond the scope of this toy Monte Carlo. Otherwise, the scattering model in the toy Monte Carlo appears to be consistent with boomc.

## 3.2 Check of Extinction:

In this check, we simulate the cuvet as a 1-cm-diameter sphere centered at the origin. While a proper simulation of the cuvet geometry is possible, the analysis of the forward-directed light

relevant for the simulating the transmission measurements is only sensitive to the pathlength, which is approximately the same. The simulated light, generated between 200 and 400 nm in wavelength, enters the sphere along the $z$ axis. At each wavelength, the fraction of light that survives at that wavelength in the forward direction is evaluated. The results are shown in Figure 12 both as a transmission fraction and an extinction length. The latter extends only to $\sim 340$ nm, the first wavelength bin where all the generated photons are recovered in the forward direction.
The toy Monte Carlo simulation is in excellent agreement up to $\sim 320$ nm where the optical model reverts to the WIN baseline model for extinction. This is expected, of course, since the transmission measurements were directly inserted into the optical model at these wavelengths.

## 3.3 Crosschecks with Excitation Measurements

For this cross check, we again simulate the 1 cm cuvets used in the excitation measurements as a 1 cm diameter sphere centered at the origin. In this case, the difference in geometry may have non-trivial effects, but there are a number of other simplifications involving the acceptance and geometry of the apparatus that probably have much larger effect.
The excitation measurements are simulated by generating light incident along the $z$ axis with a flat spectrum between 200 and 400 nm. For light observed outside of the forward direction at six output wavelengths (295, 300, 310, 320, 330 and 340 nm, corresponding to the actual excitation measurements), the distribution of input wavelength is obtained, resulting in a simulated excitation measurement. The results are shown in Figure 13, where the simulated results from the default fluorescence model are shown in blue and the data are shown in black. The green and red curves represent two variants of the default model. The toy Monte Carlo distributions are normalized by the same arbitrary factor to bring them in rough agreement with the measurements.
In the toy Monte Carlo distributions, the peak at the incident wavelength results from scattering, where the wavelength is conserved in the process. Unfortunately, the normalization of these peaks cannot be compared to the data, where they have a component from reflection off the quartz windows of the cuvet that is not simulated in the toy Monte Carlo.
At short output wavelengths (295-310 nm), a sharp decrease in the fluorescence rate is observed between 280 and 290 nm in the data. The simulations which incorporate this feature in the optical model, (green and blue curves), reproduce this edge. The red curve, which follows the 340 nm excitation curve in this range (which does not exhibit this feature), does not fall as precipitously. For the green and blue curves, however, this feature appears at all output wavelengths, whereas in the data, it gradually fades away with increasing output wavelength; it is not possible to consistently describe all the excitation data with one model, but the default model appears to be a reasonable compromise. Again, it would not be too meaningful to exactly match the measurements, since there are many geometric and optical effects in the data that have not been simulated.

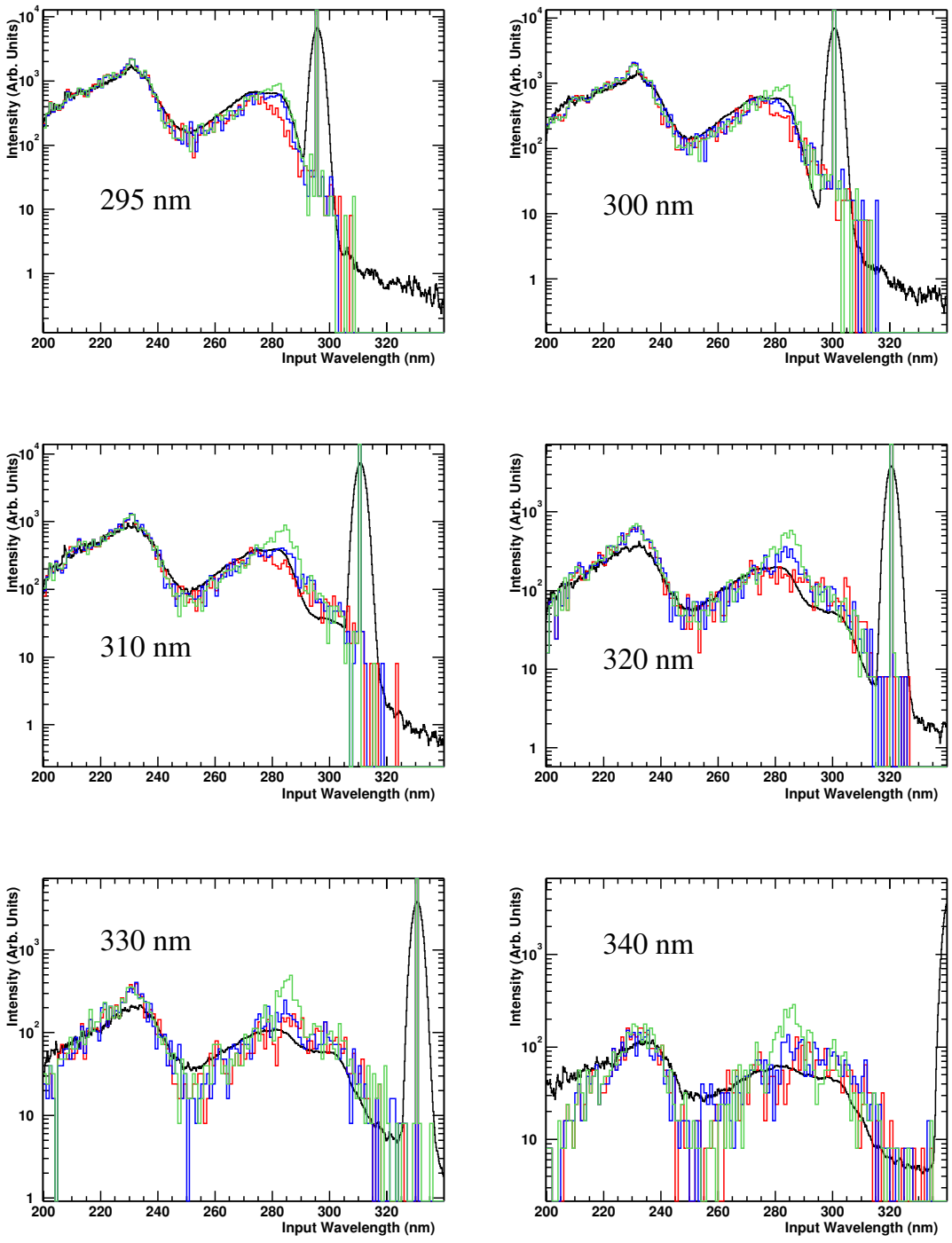


Figure 13: Comparison of toy Monte Carlo predictions for excitation curves with three fluorescence models (default (blue) and two alternative models (red and green)) to excitation data (black).

# 4 Time Spectrum of

# 5 Effective Fluorescence Spectrum

# 6 Acknowledgments

# References

[1] Various communications via Eric Hawker and Gerry Garvey from Anna Pla and Shannon.

[2] H.O. Meyer, BOONE Tech Note 90

[3] E.A. Hawker *et al.* BOONE Technical Note 31

[4] J.F. Raaf *et al.* "Mineral Oil tests for the MiniBooNE Detector"

[5] S.J. Brice *et al.* BOONE Technical Note

[6] P. Ockerse *et al.* BOONE Technical Note 74

[7] G. Garvey, private communications

[8] Jackson, J.D., *Classical Electrodynamics*.

[9] H.O. Meyer, BOONE Tech Note 114

[10] P.D. Meyers, private communications

# A Novosibirsk Function

The Novosibirsk function is given by:

$$\begin{aligned} f(x) &= \frac{1}{\sqrt{2\pi\sigma^2}} e^{-\frac{1}{2}\frac{\log^2 \Delta}{\tau^2} + \tau^2} \\ \Delta &= 1 + \frac{\sinh(\tau\sqrt{\log 4})}{\tau\sqrt{\log 4}} \frac{x-\mu}{\sigma} \end{aligned} \tag{7}$$

where $\mu$ is the peak, $\sigma$ is the width and $\tau$ is the tail parameter. For $\tau < 0$, the tail is on the left side of the peak, while for $\tau > 0$, it is on the right.